Nuclear Medicine Artifacts

SCPMG Medical Imaging Technology & Informatics
Medical Physics Group
Brian Helbig, MS, DABR

Symmetric energy windows

Intrinsic uniformity, ^{99m}Tc, 30 million counts each image, no contrast enhancement of images, acceptance testing.

Dynamic clinical study – Energy peak shift – Electrical grounding problem

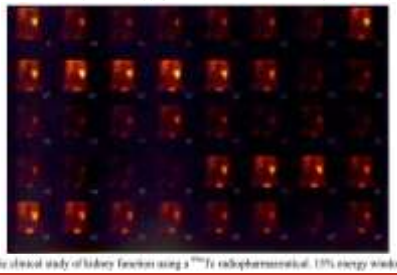

Dynamic clinical study of kidney function using a ^{99m}Tc radiopharmaceutical. 15% energy window.

Asymmetric window

Schematic representation of asymmetric energy windows

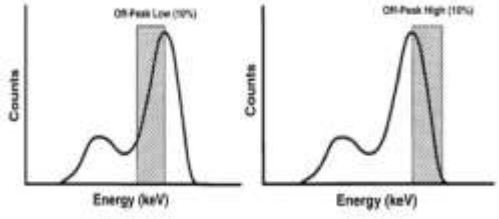

Symmetric/Asymmetric energy windows - Poor PMT balance and crystal hydration

Four million counts were acquired in each of the four intrinsic (collimator removed) QC images. Images with asymmetric windows were acquired in order to check PM tube balance and whether there was any hydration of the crystal.

TL: 20% symmetric energy window, approximately 30 000 counts.
TR: 20% symmetric energy window, approximately 75 000 counts.
BL: 10% asymmetric high energy window.
BR: 10% asymmetric low energy window.

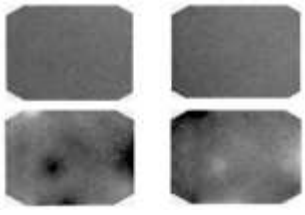

Asymmetric energy window – fault in energy correction map

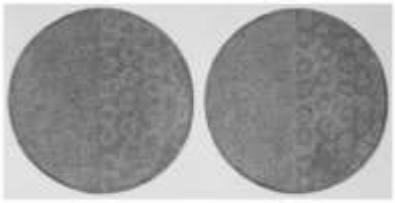

Medical Imaging Technology & Informatics (MITI)
Southern California Permanente Medical Group
7

Asymmetric energy window – clinical example with I-123 and Tc-99m

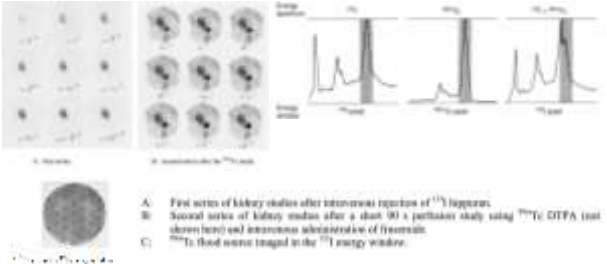

A: First series of kidney studies after intravenous injection of ^{123}I hippuran.
B: Second series of kidney studies after a short 90 s perfusion study using ^{99m}Tc DTPA (not shown here) and intravenous administration of furosemide.
C: ^{99m}Tc flood source imaged in the ^{123}I energy window.

Medical Imaging Technology & Informatics (MITI)
Southern California Permanente Medical Group
8

Clinical example - Tl-201 uniformity - Defective linearity correction

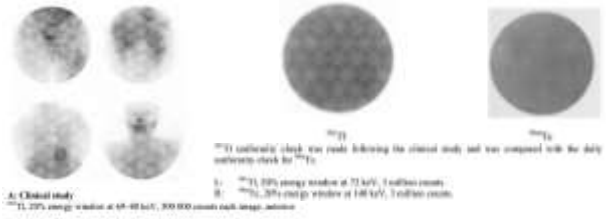

Medical Imaging Technology & Informatics (MITI)
Southern California Permanente Medical Group
9

Uniformity – Ga-67 – Separate and sum of energy windows

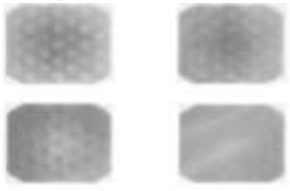

Image without linearity or energy corrections

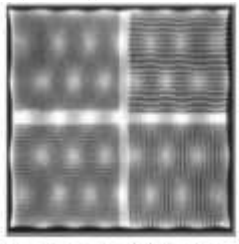

Four quadrant bar patterns, intrinsic uniformity, ^{99m}Tc, 4 million counts.

Side-by-side comparison with and without uniformity corrections

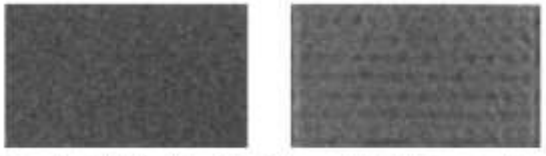

Extrinsic uniformity, LEHR collimator, ^{99m}Tc, 15% energy window, 4 million counts each image; linearity and energy corrections have been applied.

L: Uniformity obtained after application of a uniformity correction map.
R: Uniformity obtained without the uniformity correction map.

Fault energy correction map – Clinical study

Patient study of ^{99m}Tc monoclonal antibody distribution in the lower abdomen immediately after a hardware energy calibration was performed. Anterior view, LEHR collimator, 20% energy window

Loss of hermetic seal/optical coupling

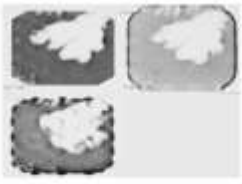

This normal 4-million count daily QC flood from one detector of a dual head system.

TL. Image acquired with the detector facing downward and with the uniformity correction activated.
TR. Image acquired with the uniformity correction map (concentrated ovals) circled turned off but with the energy and linearity corrections operating.
BL. Image showing the effect of rotating the detector so that it faced upward.

Cracked crystal – Puncture/impact

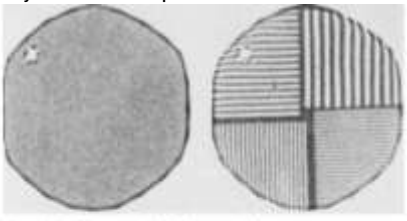

Intrinsic tests, ^{99m}Tc, 20% energy window, 3 million counts each image

1. Uniformity image.
2. Resolution image obtained with a quadrant bar pattern

Cracked crystal – Puncture/impact

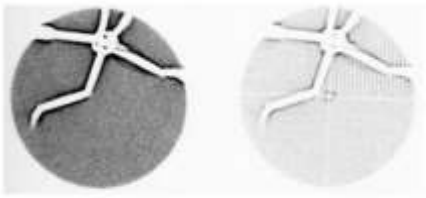

These routine uniformity (L) and spatial resolution (R) images show large, cold zigzag cracks with hot edges. This was caused by impact on the crystal. The camera is unusable until the crystal is replaced.

Cracked crystal - Thermal

Crystal hydration

A set of analogue images was acquired as part of a QC programme. A ^{99m}Tc point source was used to acquire 1.25 million counts in each image.

TL: Count rate ~10 000 counts/s, symmetric energy window.
TR: Count rate ~75 000 counts/s, symmetric energy window.
BL: Asymmetric energy window set high.
BR: Asymmetric energy window set low.

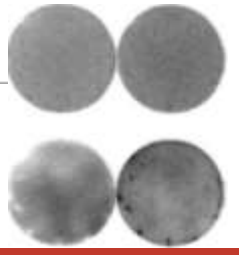

Crystal Irregularities

Acceptance testing, intrinsic uniformity, 15% symmetric energy window, 30 million counts.

A: Smoothed uniformity image.
B: Photograph of part of the crystal taken after it had been removed for replacement. A strong was shone into the crystal in order to illuminate its structure.

Uniformity – Defective PM Tube

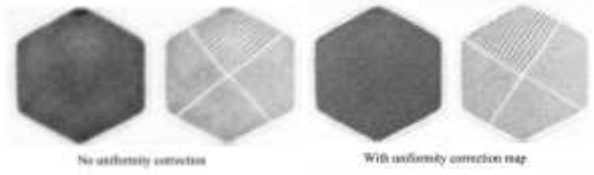

No uniformity correction

With uniformity correction map

Uniformity – Defective PM tube (newer digital camera)

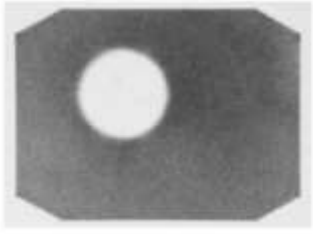

^{99m}Tc, 15% energy window, 10 million counts, modern camera.

Defective PMT at FoV edge

^{99m}Tc, 15% symmetric energy window, 256 × 256 matrix, 10 million counts.

Clinical bone scan – defective PM tube

Bone scan of patient using ^{99m}Tc phosphonate, 15% energy window

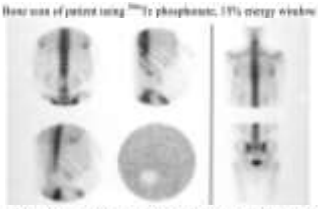

TL, TM and BL: Camera A — different single spot views of the skeleton: posterior, right anterior and right anterior oblique, respectively.
BM: Camera A — flood field image taken after the spot views.
TR and BR: Camera B — posterior spot views of the same patient.

Maladjusted PM tube

Routine intrinsic uniformity, ^{99m}Tc, 15% energy window, 128 × 128 matrix. The image has been contrast enhanced.

Unacceptable extrinsic floods – Low energy collimator misalignment

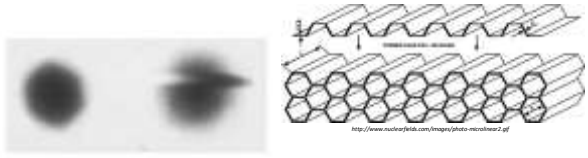

LEAP LEHR

Round FOV camera. The left image from the LEAP collimator shows a satisfactory response. The LEHR collimator (right) shows a distinct streak artefact due to hole misalignment with respect to the crystal face. This collimator requires replacement. These images were acquired at acceptance testing.

Unacceptable extrinsic floods – Low energy collimator angulation

LEAP LEHR

L: The LEAP collimator shows no abnormality in the image of the distant point source.
R: The striped response in both x and y directions indicates severe collimator hole angulation problems at manufacture, i.e. the axes of the holes are not parallel to one another and perpendicular to the surface of the collimator. This collimator is unacceptable and requires replacement.

Unacceptable extrinsic flood – Collimator septa damage - Puncture

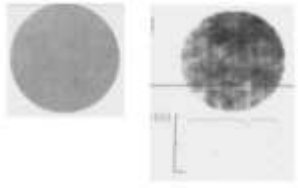

L: Analogue uniformity image.
R: High contrast digital image with a profile superimposed at the level of the small cold spot in the lower right quadrant. The count profile shows a definite dip in counts corresponding to the cold spot.

Clinical example – Collimator star pattern

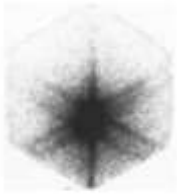

This ^{131}I image of a patient with metastatic thyroid tissue was acquired using a high energy collimator.

Fillable flood source - Air bubble

Extrinsic routine QC images using a fillable flood source, ^{99m}Tc, 20% energy window.

Uniformity image. A discrete circular cold area is seen in the middle of the FOV. Visual inspection of the flood source revealed a large air bubble. The cold indentation at the top left edge of the FOV was also due to an air bubble.

Fillable flood source - Non-uniform mixing

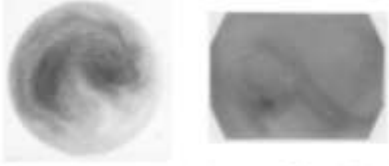

Two different examples of a routine extrinsic uniformity image using ^{99m}Tc in a fillable flood source. In each situation the ^{99m}Tc was injected into the water in the flood source and was left to disperse over a period of about one hour.

Results: The non-uniformity shown that dispersion was insufficient to produce a homogeneous distribution of ^{99m}Tc, and that mixing must take place. The right image also shows a small air bubble in the center of the FOV.

Fillable flood source – bulging sides

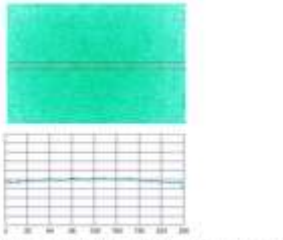

Routine uniformity image obtained with a fillable flood source. The phantom was filled with too much water, which produced bulging of the center part of the phantom.

Fillable flood source – Adherence of activity to the container at the filling site (algae)

The circular fillable flood phantom was upended to enable radioactivity to be added to the water already within the phantom. The water level was well below the filling hole. Since ^{99m}Tc pertechnetate was not available, ^{99m}Tc MDP was used and was injected with a syringe in a steady stream against the side of the phantom into the water. After removal of air and mixing, flood field uniformity images were obtained (20% energy window, 3 million counts each image). The images show the phantom in two different orientations.

Non-Uniformity in Cobalt Sheet Source

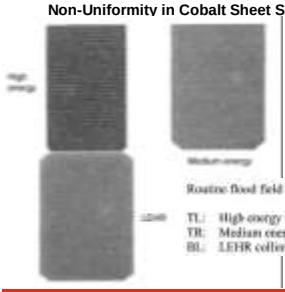

Routine flood field images from different collimators using a ^{57}Co sheet source.

TL: High energy collimator.
TR: Medium energy collimator.
BL: LEHR collimator.

Point Source Geometry and multihead systems

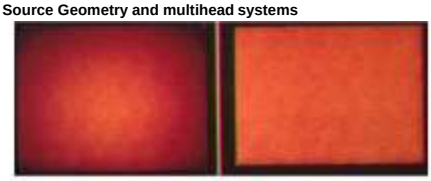

Multihead SPECT system. Intrinsic uniformity using a ^{99m}Tc point source positioned at about 50 cm centrally between the detectors in order to obtain simultaneous flood field images from each detector, 15% energy window, 30 million counts (each detector). The images are from one detector of the system.

L: Raw flood image
R: Raw image corrected for the curvature in count response (down effect).

NEMA slit pattern – Unacceptable difference in x and y spatial resolution

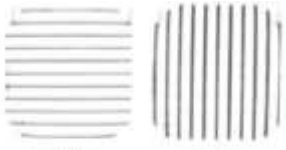

↑ Spatial resolution in *y* direction

→ Spatial resolution in *x* direction

Intrinsic resolution images were acquired with ^{99m}Tc and a NEMA slit pattern (1 mm wide slits in a sheet of lead with separations of 30 mm) during acceptance testing. ^{99m}Tc point source at 5 UHDV distance, 15% window, 3 million counts each image.

L: Slit pattern positioned for assessment of spatial resolution in the *y* direction.
R: Slit pattern rotated by 90° for assessment in the *x* direction.

Intrinsic spatial resolution - Faulty linearity correction

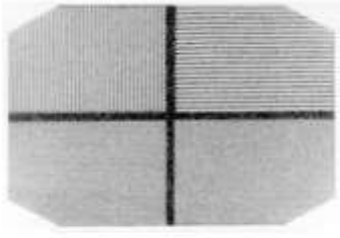

Intrinsic spatial resolution and linearity check, low-energy collimator, four quadrant bar pattern, ^{99m}Tc point source, 3 million counts.

Extrinsic Spatial Resolution - Moiré pattern

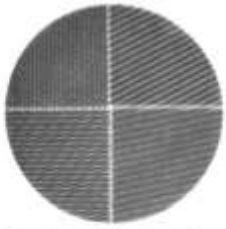

Extrinsic spatial resolution using a four quadrant bar pattern, medium energy collimator, ^{99m}Tc flood source, 15% energy window, 5 million counts. The pattern was at 7.5 cm distance from the collimator.

Uniformity and High Count Rates

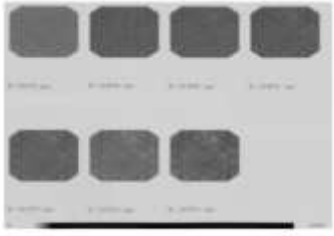

Intrinsic ^{99m}Tc images of 4 million counts were acquired with a 20% energy window for different source activities, producing different count rates.

Poor spatial resolution at high count rates due to misplaced events

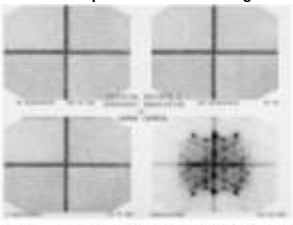

TL: 0.74 MBq (20 μCi), 365 s.
TR: 7.4 MBq (200 μCi), 60 s.
BL: 74 MBq (2 mCi), 13 s.
BR: 740 MBq (20 mCi), 749 s.

Series of intrinsic resolution images obtained at increasing count rates. The point source activity used has been increased by a factor of 10 between successive images. Each image consists of 1 million counts.

SPECT Uniformity – simulation with no noise – Effect of projection sampling

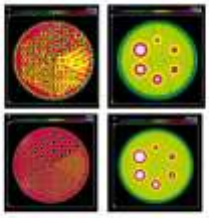

Top row: 64 x 64 matrix, 64 projections, 1 - rods, R- spheres (pixel size 3.85 mm).
Bottom row: 128 x 128 matrix, 128 projections, 2 - rods, R - spheres (pixel size 1.92 mm).

Simulations of a Data Spectrum Deluxe ECT phantom (Jaszczak phantom) with no statistical noise, 37 cm FOV with 1.5 zoom, 360° total angle of rotation, circular orbit. Reconstruction with a ramp filter and FHP, no attenuation correction. Perfect uniformity.

Comparison of high and low count densities

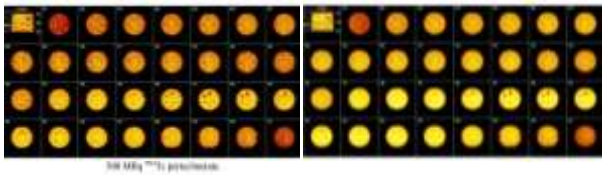

500 MBq ^{99m}Tc pertechnetate.

Acquisition: 15% energy window, high resolution collimator, 360° total angle of rotation, 60 projections, 64 x 64 matrix, 30 000 and 500 000 counts per projection.

Reconstruction: Butterworth filter and FHP, with attenuation correction.

Top images: Transverse slices from 30 000 counts per projection (1 million counts total).
Bottom images: Transverse slices from 500 000 counts per projection (30 million counts total).

Single head SPECT uniformity – Ring artifact from real data

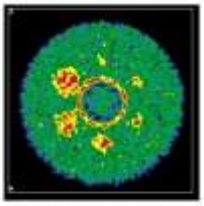

Single head SPECT, Data Spectrum ECT phantom (Jaszczak phantom), 360° total angle of rotation, reconstructed using ramp filter and FHP, with attenuation correction. Note that no smoothing filter has been applied. Transverse slice through the spheres of the phantom.

Dual head SPECT – Clinical partial ring artifact

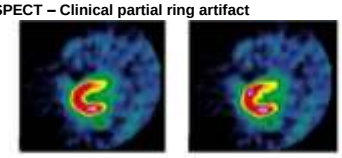

This example demonstrates the subtleties of the effect of planar non-uniformity in clinical SPECT results. Transaxial slices from a clinical ^{201}Tl myocardial perfusion study. Dual head SPECT system.

Acquisition: 180° total angle of rotation, each head rotated through 90°, 64 × 64 matrix size.

Reconstruction: FBP with a Parzen window cut-off at 1 Nyquist.

L: Transaxial slice with no simulated non-uniformity.
R: Transaxial slice with a simulated non-uniformity in one detector, consisting of a 3 pixel wide, ~10% planar non-uniformity introduced at 10 pixels from the centre of the FOV.

SPECT non-uniformity from high temperature

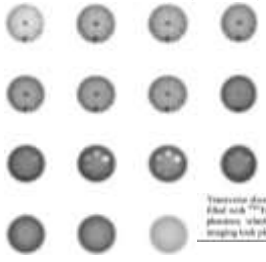

Transverse slices (no attenuation correction) from a Data Spectrum ECT phantom (Jaszczak phantom) filled with ^{99m}Tc pertechnetate. A large amount of activity of ^{99m}Tc was injected into the water filled phantom, which was then left overnight so that the radioactivity could disperse naturally before imaging took place the next day. A series of the SPECT transaxial slice images are shown.

SPECT non-uniformity from outdated uniformity corrections

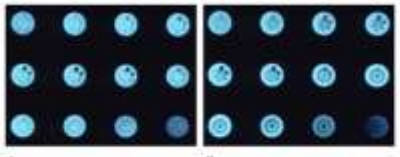

A B

Single head SPECT system, LEHR collimator, periodic check of SPECT uniformity using a Data Spectrum ECT phantom (Jaszczak phantom), ^{99m}Tc, SPECT acquisition using a 360° total angle of rotation, 64 × 64 matrix, 60 projections, reconstruction of transverse slices using a Hann smoothing filter with 1 Nyquist cut-off, FBP and Chang attenuation correction.

A: Data reconstructed with no uniformity correction.
B: Data reconstructed with a high count uniformity correction map that was about two weeks old.

Myocardial Perfusion SPECT – With and without uniformity defect

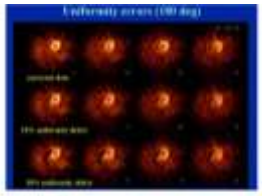

Center of Rotation (COR) Offset

Simulated reconstruction of a point source with different COR errors. Acquisition: 37 cm FOV with 1.5 zoom, 64 × 64 matrix, 360° total angle of rotation, 64 projection angles, circular orbit. Reconstruction into transverse slices using a ramp filter and FBP. No correction was made for the COR offset error. Pixel size 3.85 mm.

TL: 0 pixel offset (perfect data).
TM: 0.25 pixel offset error.
TR: 0.5 pixel offset error.
BL: 1 pixel offset error.
BM: 1.5 pixel offset error.
BR: 2 pixel offset error.

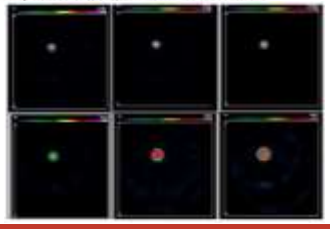

Clinical SPECT brain perfusion – Effect of COR offset

Single head SPECT system, normal ^{123}I IMP brain perfusion SPECT study, 360° total angle of rotation, 64 × 64 matrix. Data were collected and reconstructed by FBP into a single reconstructed transverse slice with four different COR offsets.

TL: 0 pixel offset.
TR: 0.5 pixel offset.
BL: 1.0 pixel offset.
BR: 2.5 pixel offset.

Effect of detector head tilt - Myocardial perfusion study

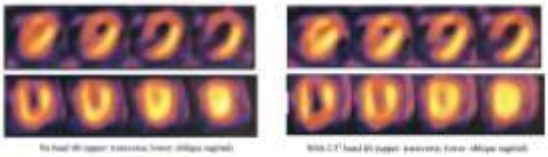

Effects of color table – Myocardial perfusion

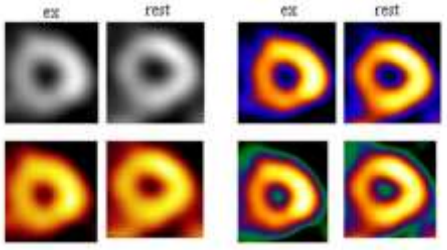

Whole body Scan – Faulty PM tube old linearity and energy corrections

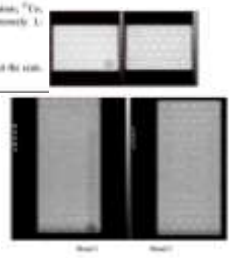

Whole body scan – Co57 versus Tc-99m energy window

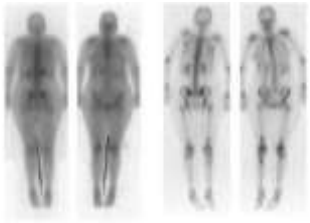

Medical Imaging Technology & Informatics (MITI)
Southern California Permanente Medical Group
52

Whole Body Scan – Contamination on handkerchief

Whole body scan three days after administration of a therapeutic amount of ^{131}I iodide.

L: Anterior view.
R: Posterior view.

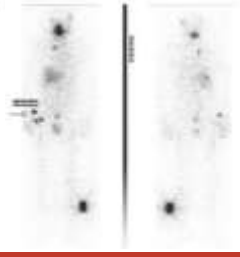

Medical Imaging Technology & Informatics (MITI)
Southern California Permanente Medical Group
53

Gated SPECT acquisition – Problems due to heart arrhythmia

Gated SPECT data acquisition of myocardial perfusion (from a three head SPECT system) using: a fixed acquisition time per projection of 45 s and fixed time bins for the gating; a beat acceptance window of ±25% of the average beat length (determined just prior to data acquisition); a 64 × 64 matrix and 60 projections.

L: One projection image (summed bins).
M: Sinogram from the profile limits shown on the left.
R: Compressed image from the same profile limits.

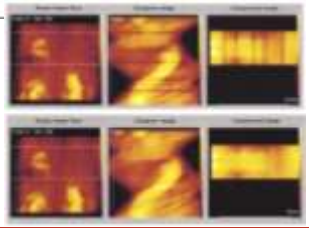

Medical Imaging Technology & Informatics (MITI)
Southern California Permanente Medical Group
54

System uniformity – Contaminated collimator

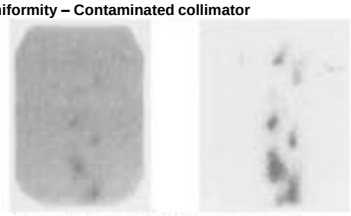

L: Uniformity image, 15% window, ^{99m}Tc, LEAP collimator, 5 million counts.
R: Background image taken immediately after the uniformity image with the same acquisition time.

Results: The dark patches seen in the uniformity image are due to radioactive contamination, as shown in the background image.

Positron range and image quality

^{18}F ^{68}Ga ^{124}I

FIG. 2.4 The Jaka brain phantom was filled with three different radiotracers (from left to right, ^{18}F, ^{68}Ga and ^{124}I) labelled with positron emitters. The maximum positron energy for these three radionuclides is 0.6, 1.9 and 4.6 MeV, respectively. The phantom was imaged on a dedicated brain-only PET system with 3 mm LSO (lutetium oxyorthosilicate) based crystals. The increased blurring for ^{68}Ga and ^{124}I compared to the low energy positron emitter ^{18}F should be noted.

PET detector failure

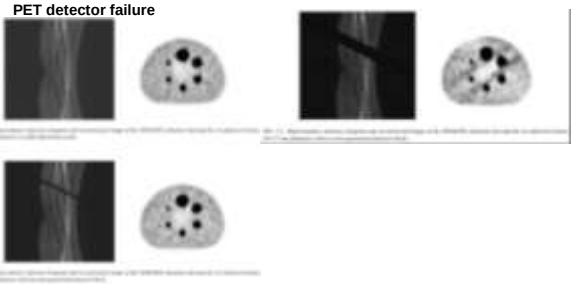

Controller board failure

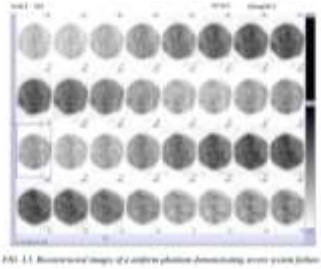

Faulty timing calibration

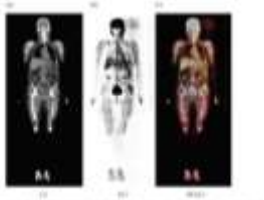

Memory board failure

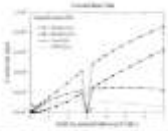

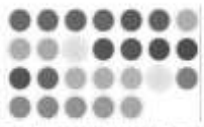

Normalization

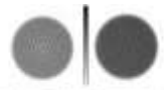

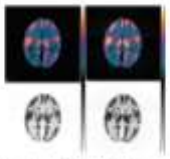

Faulty normalization

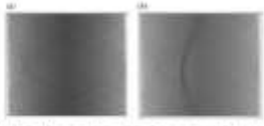

Scatter correction artifact

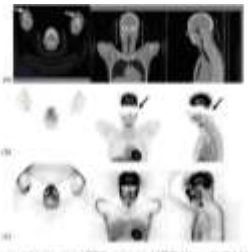

Scatter correction artifact

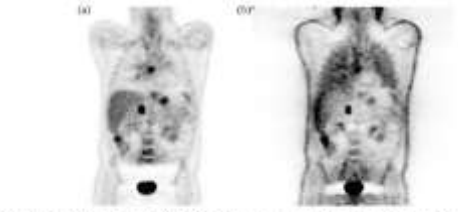

FIG. 1.23. Coronal images of a whole body NDG-PET scan with attenuation and scatter correction (a) and without correction (b). Increased photopenic areas around the bladder on the corrected image should be noted.

Intravenous contrast artifact

Intravenous contrast artifacts

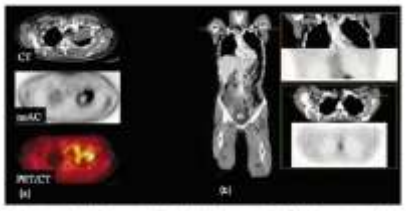

FIG. 1.24. (a) Contrast enhanced CT, uncorrected PET, and PET/CT fusion using AC-PET data demonstrating a hot spot artifact from focal contrast accumulation in the subclavian vein. (b) The use of a modified intravenous contrast administration protocol can help to reduce contrast accumulation in the subclavian vein while providing generally good contrast enhancement. AC: attenuation corrected; no AC: not attenuation corrected.

Breathing motion artifact

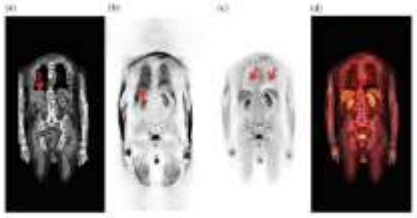

Subcutaneous tracer infiltration

FIG. 4.2 Whole body FDG-PET/CT demonstrating subcutaneous infiltration in the left arm following tracer administration.

Contamination at injection site

Contamination during flushing

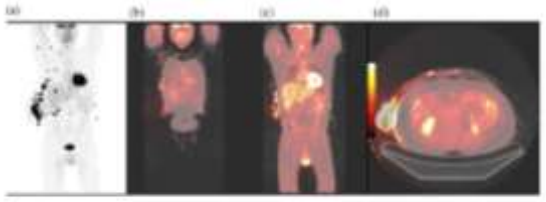

FIG. 4.8. Extensive contamination seen on maximum intensity projection PET and localized to extra-corporeal foci only on fused AC-PET/CT images. (a) Maximum intensity projection; (b) and (c) two selected coronal slices; (d) a transaxial slice through the contamination site.

Contamination post injection

FIG. 4.9. Whole body AC-PET image demonstrating a bending artefact resulting from a left side contamination of the patient's clothes following radiotracer administration. The truncation artefact in the proximal arms should also be noted (see Section 3.8).

Data entry errors and SUV analysis

TABLE 4.1. EFFECT OF VARIATION IN PATIENT ENTRIES (WEIGHT, UNITS, DOSE AND INJECTION TIME) ON MAXIMUM STANDARDIZED UPTAKE VALUE (SUV_{max}) MEASUREMENTS

Weight	Units	Dose (MBq)	Injection time	SUV_{max}
100	kg	350	14:00	4.0
90	kg	350	14:00	4.5
200	lb	350	14:00	2.3
100	kg	400	14:00	3.9
100	kg	350	15:00	3.3

Insufficient Bed Overlap

Thank you for your attention!

References

INTERNATIONAL ATOMIC ENERGY AGENCY, PET/CT Atlas on Quality Control and Image Artefacts, IAEA Human Health Series No. 27, IAEA, Vienna (2014).

INTERNATIONAL ATOMIC ENERGY AGENCY, IAEA Quality Control Atlas for Scintillation Camera Systems, IAEA, Vienna (2003).